Clinical Image Quality Assessment of Accelerated Magnetic Resonance Neuroimaging Using Compressed Sensing

Samir D. Sharma, PhD,† Caroline L. Fong, MD,‡ Brian S. Tzung, MD,§ Meng Law, MD,|| and Krishna S. Nayak, PhD†*

Purpose: The aim of this study was to determine to what degree current compressed sensing methods are capable of accelerating clinical magnetic resonance neuroimaging sequences.

Methods: Two 2-dimensional clinical sequences were chosen for this study because of their long scan times. A pilot study was used to establish the sampling scheme and regularization parameter needed in compressed sensing reconstruction. These findings were used in a subsequent blinded study in which images reconstructed using compressed sensing were evaluated by 2 board-certified neuroradiologists. Image quality was evaluated at up to 10 anatomical features.

Results: The findings indicate that compressed sensing may provide 2-fold acceleration of certain clinical magnetic resonance neuroimaging sequences. A global ringing artifact and image blurring were identified as the 2 primary artifacts that would hinder the ability to confidently discern abnormality.

Conclusion: Compressed sensing is able to moderately accelerate certain neuroimaging sequences without severe loss of clinically relevant information. For those sequences with coarser spatial resolution and/or at a higher acceleration factor, artifacts degrade the quality of the reconstructed image to a point where they are of little to no clinical value.

Key Words: compressed sensing, clinical quality assessment, accelerated imaging, magnetic resonance neuroimaging

(*Invest Radiol* 2013;48: 638–645)

Magnetic resonance imaging (MRI) is arguably the most powerful modality for neuroimaging because there is no ionizing radiation and it provides 3-dimensional (3D) coverage with high spatial resolution and a variety of contrast mechanisms that allow for tissue characterization and functional and advanced physiologic mapping.[1,2] Its primary limitations are related to tradeoffs between speed, spatial resolution, signal-to-noise ratio, and image artifacts.

In this work, we explored the use of a new approach called compressed sensing (CS) that may allow magnetic resonance neuroimaging to overcome these limitations. Compressed sensing requires that (*a*) k-space is undersampled in such a way that the resultant aliasing artifacts are incoherent and (*b*) the image to be reconstructed can be represented by relatively few nonzero terms in a known (eg, wavelet, discrete cosine) transform.[3,4] If these 2 requirements are met, then a nonlinear reconstruction can be used to recover the image from undersampled k-space measurements.

The theory underlying CS[3,4] suggests that magnetic resonance (MR) data acquisitions may be shortened by orders of magnitude without a significant loss of image quality. Lustig et al[5] laid the foundation for CS in MRI. Others have built upon this framework, generally achieving 2× to 5× acceleration.[6–8] Vasanawala et al[9] showed that 4× acceleration of 3D clinical pediatric MRI sequences could be achieved by using this technique. These results favor the adoption of CS in routine clinical MRI examinations, especially for high-resolution 3D brain scans.[10,11]

Whereas previous MRI acceleration techniques, such as parallel imaging or echo-planar and spiral sampling, produce either noise amplification[12,13] or image artifacts[14,15] that are well understood, the effects of CS on clinical image quality remain an open question. To begin toward an answer, the artifacts arising in CS images must be identified and characterized by radiologists. This analysis shall provide insight into the use of this method as well as the potential to integrate CS with other acceleration techniques, such as parallel imaging.

The objective of this study was to determine to what degree conventional CS methods are capable of accelerating current clinical magnetic resonance neuroimaging sequences. Neuroimaging was chosen because it accounts for roughly 35% of all clinical MRI scans, and accelerating such protocols will have the immediate potential to increase patient throughput and reduce health care costs. This is especially relevant given the marked growth in MRI examinations in the past decades. A robust technique that would allow faster imaging with diagnostic quality images would improve patient access to MRI examinations. Faster time of imaging would mean less wait time for patients to receive their MRI scan and better patient care.

The study began with an iterative process in which neuroradiologists assessed CS-reconstructed images to establish sampling and reconstruction parameters as well as develop insight into image artifacts. Subsequently, a blinded clinical qualitative assessment of CS-reconstructed images was performed for 2 routine clinical sequences and 3 acceleration factors. This study provides a new clinical perspective on the value of CS methods in accelerating magnetic resonance neuroimaging while also developing an understanding about the CS-related artifacts that would complicate diagnostic accuracy.

METHODS

Implementation of Compressed Sensing

In CS-MRI, design choices must be made in both data acquisition and image reconstruction. In partial k-space CS acquisitions, subsampling occurs only along the phase-encoding axes because no time savings are realized by reducing the number of readout samples for a specified spatial resolution. The phase-encoding axes are sampled with variable density so that central k-space, which contains most of the energy of MR images, is more heavily sampled than the periphery. Figure 1 shows 2 example sampling schemes, each drawn from a separate sampling density. Sampling density A decays with polynomial power $p = 2$, whereas sampling density B decays with polynomial power $p = 6$. The thick solid line denotes the sampling density, whereas the thin lines show which phase-encoding lines would be sampled in 1 of many possible realizations. Both of these schemes result in 2× acceleration of a 2D data acquisition. That is, one-half of the

Received for publication October 19, 2012; and accepted for publication, after revision January 26, 2013.

From the *Department of Radiology, University of Wisconsin, Madison; †Ming Hsieh Department of Electrical Engineering, University of Southern California; ‡Department of Radiology, Kaiser Permanente, Los Angeles; §Department of Radiology, Renaissance Imaging Medical Associates, Northridge; and ||Department of Radiology, University of Southern California, Los Angeles, CA.

Conflicts of interest and sources of funding: none declared.

Reprints: Samir D. Sharma, PhD, Department of Radiology, University of Wisconsin, 1111 Highland Ave, Madison, WI 53705. E-mail: sdsharma2@wisc.edu.

ISSN: 0020-9996/13/4809–0638

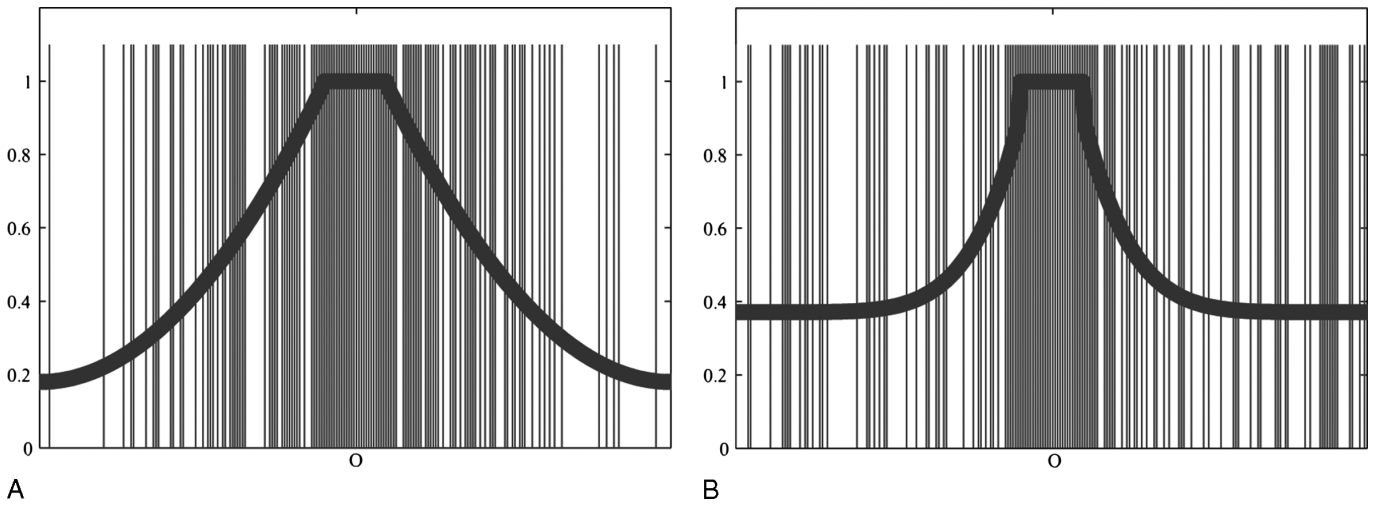

FIGURE 1. Two 1D sampling densities. The bold line denotes the sampling density, and the thin lines denote which of the 256 phase encodes would be sampled in 1 of many possible realizations. Both densities sample the 25 central k-space phase encodes, and both result in 2× acceleration. A, Sampling density with polynomial decay rate of $p = 2$, referred to as sampling density A. B, Sampling density with polynomial decay rate of $p = 6$, referred to as sampling density B.

available samples on a 2D grid would be acquired by either of these sampling schemes. For image reconstruction, one must also select the sparsifying transform and the regularization parameter. A detailed discussion of these 2 choices appears in later sections.

Data Collection

Raw k-space data were collected from 15 patients scheduled for routine MRI on a 3-T Signa EXCITE HDxt system (GE Healthcare, Waukesha, WI) using a protocol approved by the local institutional review board. Two sequences from the seizure/epilepsy clinical protocol were chosen for this study because of their long scan times: (1) 512 × 346 × 28 2D multislice oblique-coronal T2-weighted spin-echo (T2-SE) with an echo time/repetition time of 102/6367 milliseconds, echo train length of 15, and a scan time of 4 minutes 10 seconds and (2) 320 × 192 × 28 2D multislice oblique-coronal T2-weighted fluid-attenuated inversion recovery (T2-FLAIR) with an echo time/inversion time/repetition time of 150/2200/8900 milliseconds and scan time of 5 minutes 12 seconds. The T2-FLAIR is a workhorse sequence in neuroimaging protocols because most of the pathology in the brain is best seen with this sequence. No changes were made to the clinical settings, and these sequences did not use parallel imaging. The body coil was used for radiofrequency transmission and an 8-channel head array coil was used for signal reception.

Image Reconstruction

The fully sampled k-space measurements were downsampled using the 2 variable-density schemes in Figure 1 to simulate an accelerated data acquisition. The central 10% of the phase-encoding lines were sampled in both instances. These 2 schemes were chosen because of the significant difference of the sampling density at the higher spatial frequencies. Of interest was observing how this difference would affect perception of image quality. For a specified sampling density, 10,000 sampling realizations were generated and that which minimized the maximum sidelobe magnitude of the point-spread function was selected as a candidate sampling pattern.[5] The min-max criterion was chosen in an effort to suppress the incoherent aliasing interference in the reconstructed image. This procedure was performed for 2×, 3×, and 4× acceleration factors. The k-space data were normalized by the maximum pixel value of the zero-filled density-compensated image to mitigate the effects of unknown quantities, such as transmit and receive gain factors, when selecting the regularization parameter. Images were reconstructed via minimization of the convex expression in Equation 1. In this expression, x is the image to be recovered, Ψ represents the sparsifying transform (eg, Daubechies-4 [DB-4] wavelet transform), Φ_u is the undersampled Fourier transform matrix, and s denotes the subsampled k-space data. The user-tuned regularization parameter λ weights relative importance between data fidelity and transform coefficient sparsity.

$$\min_{x} \underbrace{\|s-\Phi_u x\|_2^2}_{\text{data fidelity}} + \underbrace{\lambda\|\Psi x\|_1}_{\substack{\text{transform}\\ \text{sparsity}}} \quad (1)$$

The reconstruction was implemented in Matlab (The Mathworks, Inc, Natick, MA) via the nonlinear conjugate gradient method. The DB-4 wavelet transform was used as the sparsifying basis.[16] Images were reconstructed independently for each of the 8 receiver channels and the results were combined using root-sum-of-squares (RSS).[17] This focused the study on CS by excluding any potential benefits from parallel imaging.

Study Design

Figure 2 shows a flowchart of the study design, which consists of 2 parts: (1) a pilot study to establish an appropriate sampling pattern and regularization parameter and (2) a blinded study to assess the quality of CS-reconstructed brain images using the settings established in the pilot study. In both studies, images were reviewed by 2 board-certified neuroradiologists. The following sections explain each study in greater detail.

Pilot Study

The goal of the pilot study was to establish the sampling pattern and regularization parameter for each of the 2 sequence and 3 acceleration rate pairs. Five data sets from the collection of 15 were used for this study.

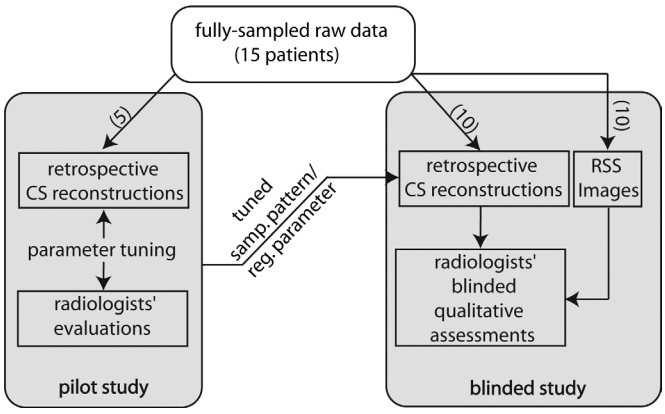

FIGURE 2. The study design was divided into 2 parts. The pilot study used 5 data sets from the total of 15. The goal of the pilot study was to establish the sampling pattern and regularization parameter for each sequence and acceleration rate pair as well as to identify image artifacts. Having established these settings, the goal of the blinded study was to qualitatively assess CS-reconstructed image for acceleration factors of 2×, 3×, and 4×. The remaining 10 data sets were used in this blinded study.

The readers reviewed CS-reconstructed images for each of the 2 sequences with full knowledge of the acceleration factor, sampling pattern, and regularization parameter for each image. Each reader commented on the overall image quality, identified image artifacts, and described potential misdiagnoses that may be caused by each of the artifacts. They also scored the conspicuity of the artifacts in a set of CS-reconstructed images for which they did not have knowledge of the acceleration factor, sampling pattern, and regularization parameter.

The feedback from the readers' evaluations was reviewed to update the choice of sampling pattern density and regularization parameter for each sequence and acceleration rate pair. The new regularization parameter was chosen based on observations from previous CS experiments. In total, the regularization parameter was varied between 0.0001 and 0.005. A new set of images were reconstructed from the 5 data sets and the evaluations were repeated. This iterative process continued until a consensus was reached on the sampling pattern and regularization parameter for each sequence and acceleration rate pair.

Blinded Study

The goal of the blinded study was to assess the quality of brain images reconstructed using CS. The sampling pattern and regularization parameter determined from the pilot study were used in this blinded study. From each of the remaining 10 data sets, 2 contiguous 2D k-space slices were selected for each sequence. Images were reconstructed, as previously described, from each k-space slice with acceleration rates of 2×, 3×, and 4× and by using the RSS of the fully-sampled k-space data, hereafter referred to as 1×, yielding a total of 4 images per k-space slice and 80 images for each of the 2 sequences. For each k-space slice, the 4 associated images (ie, 1×, 2×, 3×, 4×) were randomly permuted and uploaded to the Synapse Picture Archiving and Communication System (Fujifilm Medical Systems, Stamford, CT) network for blinded review. This Synapse network is the same one used for current clinical image readings. The readers scored image quality at up to 10 different anatomical features: basal ganglia, circle of Willis, gray-white junction, cerebellar structures, brainstem, subarachnoid space sharpness, hippocampus, fornix, ventricles, and red nucleus. The scoring was based on a 3-point scale: 3 = well defined, 2 = seen but not well defined, and 1 = not seen. Wilcoxon signed-rank tests were performed in Microsoft Excel (Microsoft, Redmond, WA) and Matlab to test the null hypothesis that the median qualitative scores at 1× acceleration and each of 2×, 3×, and 4× acceleration were the same. Apart from the numeric scoring, the readers also assessed the diagnostic quality of the reconstructed images.

RESULTS

Pilot Study

Sampling density B (in Fig. 1) was chosen for both sequences at all 3 acceleration rates. This density sampled more of the higher spatial frequencies than sampling density A. A regularization parameter of 0.002 was decided upon for all T2-SE sequences and for the 2× T2-FLAIR sequence, whereas a value of 0.001 was chosen for the 3× and 4× T2-FLAIR sequence.

Two primary artifacts were identified in the CS-reconstructed images: (1) a global ringing artifact and (2) the blurring of fine detail in brain structures. The ringing artifact was described as mimicking what is seen from patient motion and presumably originated from the variable-density sampling scheme. This artifact was deemed to be acceptable because it was a structured artifact that could be read through. In contrast, the blurring artifact caused a loss of image resolution, which was not tolerated because the high-resolution information and possible lesion conspicuity were lost. The selection of sampling density B, which sampled more of the higher spatial frequencies than sampling density A, reflects the tolerance for image ringing but not blurring. Furthermore, the choice of low regularization parameter reinforces the desire to avoid any sense of image blurring.

Blinded Study

Figures 3 and 4 show examples of fully sampled RSS reference and CS-reconstructed images for the T2-SE and T2-FLAIR sequences, respectively. The white arrows in the figures highlight the global ringing artifacts. Generally, the 3× T2-SE, 4× T2-SE, and 2× T2-FLAIR images suffered from mild to moderate ringing and mild blurring artifacts. The gray-white differentiation in the T2-SE images had become less apparent because of the mild blurring. Large lesions, defined as those greater than 3 cm in transverse diameter, would likely be conspicuous and characterized in these images, but detailed structures, such as those of the hippocampus, are visualized but in less detail. Figure 5 illustrates this loss of detailed structure in CS-reconstructed images. This figure shows zoom-in views of the hippocampus for the T2-SE images seen in Figure 3. The laminar architecture becomes difficult to distinguish in the 3×- and 4×-accelerated image because of blurring. Clinically, resolving subtle hippocampal anatomy is vital because this sequence is used in a seizure/epilepsy protocol. The 3× T2-FLAIR and 4× T2-FLAIR images suffered from severe ringing and blurring artifacts. Large structures such as the ventricles were blurred beyond acceptable clinical limits.

Table 1 lists the qualitative scores for the T2-SE and T2-FLAIR sequences. The results are shown for each of the up to 10 image features averaged over the 10 data sets. For the T2-SE sequence, image features such as the circle of Willis and the ventricles were judged to be nearly as well defined in the 3×-accelerated images as in the 1× image, whereas other features such as the basal ganglia and hippocampus were less conspicuous at the higher acceleration factors. The same general trend holds for the T2-FLAIR images, although the scores go much lower than their T2-SE counterparts.

Figure 6 shows a bar plot of the overall average qualitative score, which was calculated as the average of the image feature scores, for the T2-SE sequence. Figure 7 shows a similar plot for the T2-FLAIR sequence. The overall average qualitative scores, averaged over the 2 readers, decreased monotonically from 2.99 for the 1× images to

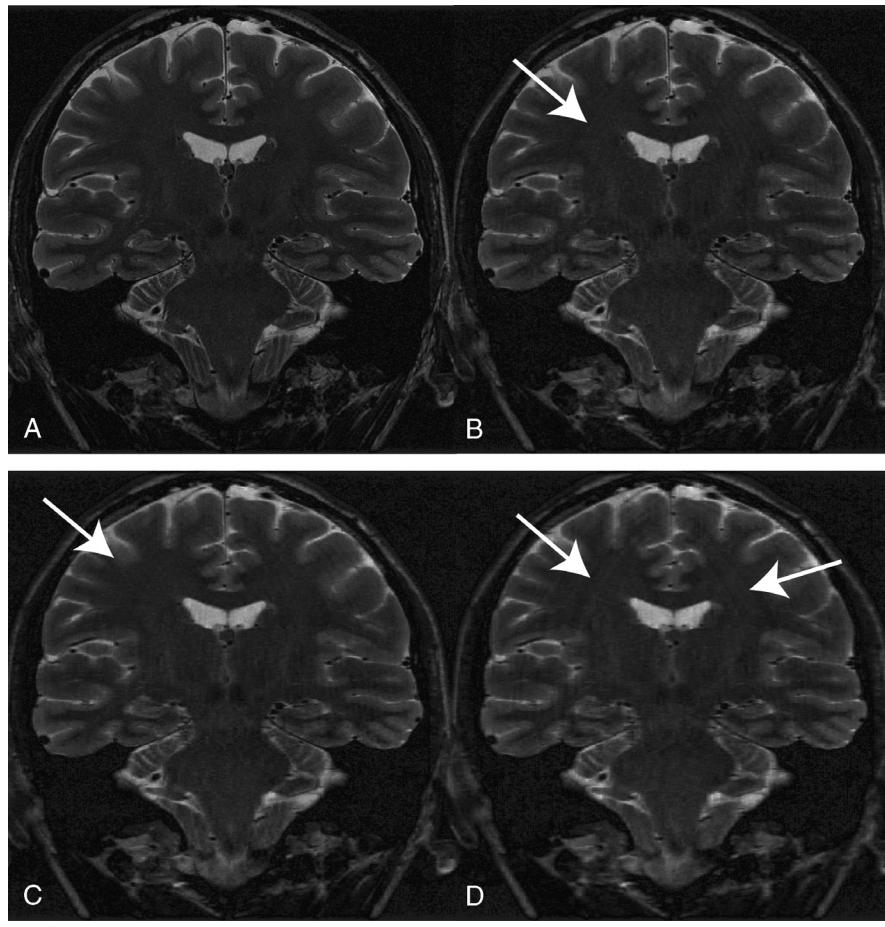

FIGURE 3. T2-SE images reconstructed using (A) fully sampled RSS; scan time is 4 minutes 10 seconds. B, 2×-accelerated CS followed by RSS; effective scan time is 2 minutes 5 seconds. C, 3×-accelerated CS followed by RSS; effective scan time is 1 minute 23 seconds. D, 4×-accelerated CS followed by RSS; effective scan time is 1 minute 3 seconds. The white arrows highlight areas in which the global ringing artifact was most apparent. There is also a slight blurring of fine-scale image features as the acceleration factor increases.

2.13 for the 4×-accelerated CS images for the T2-SE sequence and from 2.69 to 1.29 for the T2-FLAIR images. Among the CS reconstructions, only the 2× T2-SE images were considered to be of clinical diagnostic quality. The 3× T2-SE, 4× T2-SE, and 2× T2-FLAIR image sets were of some clinical diagnostic quality, whereas the 3× T2-FLAIR and 4× T2-FLAIR image sets were of little to no clinical diagnostic quality. Statistically significant differences in the medians of the qualitative scores between 1× and each of 2× to 4× were found in all cases ($P < 0.0001$).

DISCUSSION

Compressed sensing reconstruction appears to affect different anatomies in different ways within the same image. At the ventricles and circle of Willis, for example, there is little to no difference between the 1× and 2× T2-SE scores (Table 1). However, those scores at the basal ganglia and hippocampus differ quite noticeably. This discrimination of reconstruction quality may be explained by a combination of the size and/or the signal intensity of the anatomy. Large anatomical structures or structures with markedly different signal intensity from the surrounding brain, such as the ventricles or circle of Willis, respectively, remained clearly visible with increasing acceleration factor even in the presence of slight blurring. Conversely, the basal ganglia and hippocampus are smaller structures whose signal intensities in T2-weighted images are very similar to the surrounding brain parenchyma. The conspicuity of these anatomies was more noticeably affected by blurring, as reflected in their qualitative scores.

The reduction in imaging time for routine and advanced MR neuroimaging sequences has a number of advantages. Shorter imaging times will reduce both physiologic and nonphysiologic patient motion. Furthermore, the shortening of MRI protocols will provide currency to increase the field-of-view, spatial resolution, and/or number of acquisitions, thereby increasing signal-to-noise ratio and image quality.

Although the data show significant differences in the median scores between each of the degrees of compression, the definition of diagnostic images depends on visualization of T2 hyperintense signal abnormalities in the brain, especially in patients with multiple sclerosis. Both interpreters determined that although artifacts were present to an increasing degree with increased compression, the artifacts were able to be ignored for diagnostic purposes on the 2× T2-SE images. Therefore, the determination of "diagnostic image quality" was a subjective one made by the interpreters.

The significant disparity in reconstruction quality and related qualitative scoring between the T2-SE and T2-FLAIR sequences raises the question of what factors influence the clinical applicability of CS in MRI. We propose an explanation motivated by the theoretical results in CS and supported by the experimental findings. Informally, Candes

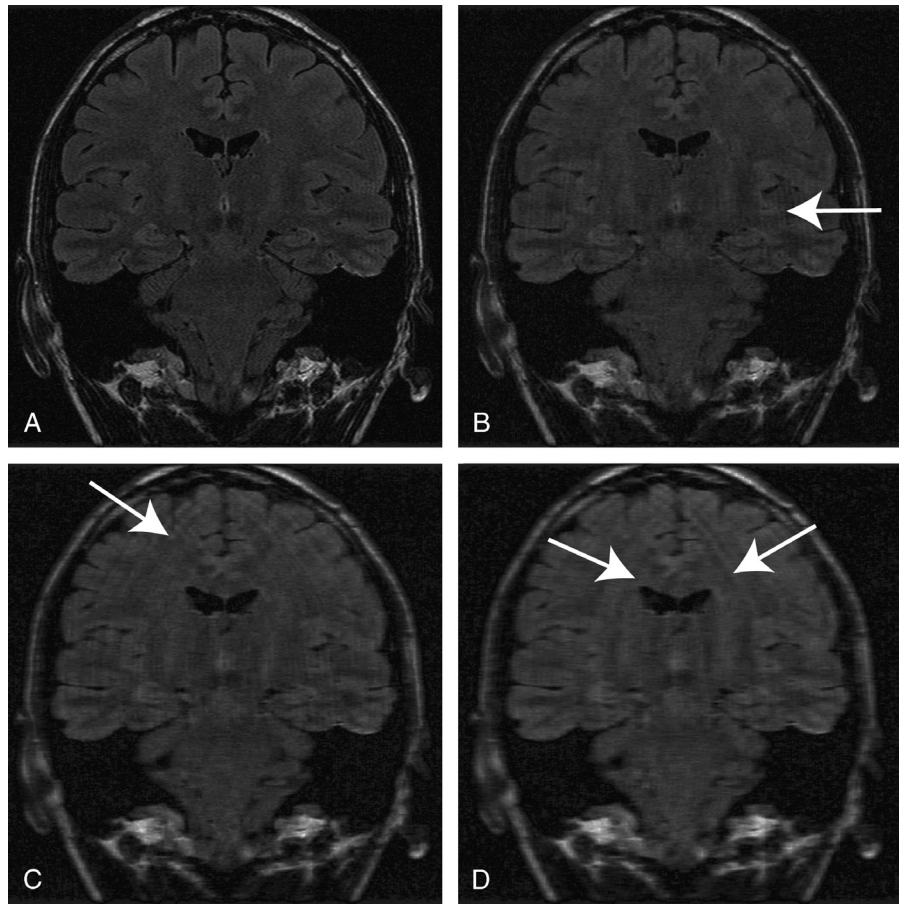

FIGURE 4. T2-FLAIR images reconstructed using (A) fully sampled RSS; scan time is 5 minutes 12 seconds. B, 2×-accelerated CS followed by RSS; effective scan time is 2 minutes 36 seconds. C, 3×-accelerated CS followed by RSS; effective scan time is 1 minute 44 seconds. D, 4×-accelerated CS followed by RSS; effective scan is time 1 minute 18 seconds. The white arrows highlight areas in which the global ringing artifact was most apparent. There is also a significant blurring of fine-scale image features as the acceleration factor increases.

and Tao[18] show that to reconstruct an image to a given fidelity, the number of required measurements is directly proportional to the number of significant coefficients in the sparsifying transform. Translating that result into this work, Figure 8 shows T2-SE and T2-FLAIR images created using only a selected fraction of the highest magnitude DB-4 wavelet coefficients. As these fractions decrease, the T2-SE image quality degrades more gracefully than does the T2-FLAIR image. The figure shows that there are relatively more

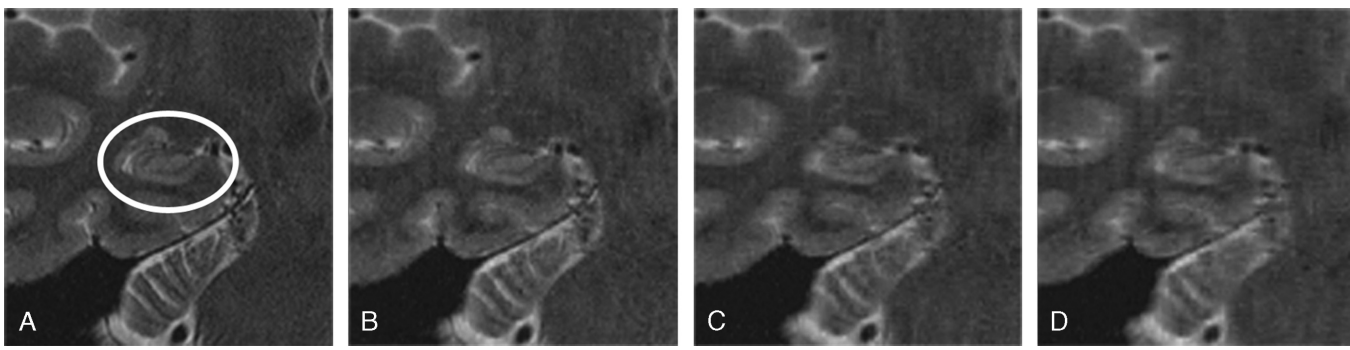

FIGURE 5. Zoom-in view of the hippocampus from the T2-SE sequence for (A) fully sampled (1×) image, (B) 2×-accelerated CS, (C) 3×-accelerated CS, and (D) 4×-accelerated CS. The hippocampus is outlined by the white ellipse. At 1× and 2×, the hippocampus is clearly visible. At 3× and 4×, artifacts in the CS-reconstructed images blur the subtle features. Resolving fine hippocampal structures in this image is important because this sequence is used for patients with epilepsy.

TABLE 1. Qualitative Scores for the T2-SE and T2-FLAIR Images

	T2-SE				T2-FLAIR			
	1×	2×	3×	4×	1×	2×	3×	4×
Ventricles	3.00	3.00	2.90	2.60	2.85	2.30	1.65	1.55
Circle of Willis	3.00	3.00	2.90	2.65	N/A	N/A	N/A	N/A
Brainstem	3.00	2.95	2.80	2.40	2.70	2.05	1.40	1.25
Red nucleus	3.00	2.70	2.55	2.35	2.90	2.35	1.75	1.70
Subarachnoid space sharpness	3.00	2.85	2.50	2.10	2.85	2.20	1.60	1.45
GW junction	3.00	2.55	2.30	2.05	2.60	1.85	1.30	1.20
Fornix	3.00	2.80	2.40	2.00	2.55	1.65	1.15	1.05
Cerebellar structures	3.00	2.75	1.95	1.70	2.50	1.60	1.30	1.15
Hippocampus	2.95	2.65	2.20	1.80	2.70	1.80	1.25	1.10
Basal ganglia	2.90	2.45	1.85	1.75	2.65	1.95	1.35	1.25

The results are shown for each of the image features, averaged over the readers, the 10 data sets, and 2 slices per data set. Scoring was based on a 3-point scale: 3 = well defined, 2 = seen but not well defined, and 1 = not seen. The rows are ordered such that large structures or structures with high contrast, such as the ventricles or circle of Willis, respectively, appear near the top, whereas smaller structures or structures with low contrast appear at the bottom. It appears that, especially in the T2-SE images, the qualitative score is dependent on either the size or the contrast of the image feature.

GW indicates gray-white.

significant transform coefficients for the T2-FLAIR image than for the T2-SE image. Thus, one would expect that a relatively more number of measurements would be needed for the T2-FLAIR sequence than the T2-SE sequence. Indeed, the findings support this expectation.

An interesting perspective emerges if absolute, rather than relative, number of measurements is considered. Figure 9 is a plot of the overall average qualitative score, averaged from the 2 readers, versus the absolute number of phase-encode lines used in the CS reconstruction. In this view, the perceived difference between the results of the 2 sequences becomes less significant. The overall average qualitative scores appear to strongly depend on the absolute, rather than relative, number of phase-encode lines used in the CS reconstruction.

Although the results of this study suggest that CS may find a role in clinical neuro-MRI, there exist barriers that must be overcome before CS-MRI will gain wide clinical acceptance. This study explored 1 particular implementation of CS, which used a specific sampling pattern for each acceleration factor, a specific sparsifying transform, and a specific reconstruction method. Our findings using this implementation are not necessarily generalizable to all types of CS implementations. A thorough understanding of how different implementations affect image quality would likely facilitate the adoption of some form of CS into clinical practice. Another question that must be addressed is the effects of a CS reconstruction on various pathologies. This study has identified what general image artifacts may hinder the conspicuity or characterization of pathology, but a thorough understanding of how they affect the ability to diagnose remains an open question. For example, it is vital that a neuroradiologist know the consequences of the image blurring artifact on various pathologies before a full-scale clinical implementation of CS. There are technical challenges

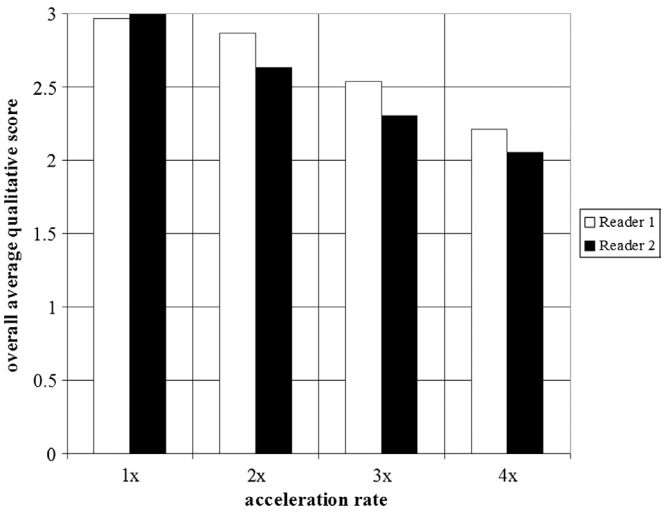

FIGURE 6. Overall average qualitative scores of the T2-SE images for each reader. The score was calculated as an average of the image feature scores, averaged over the 10 patients and 2 image slices per patient.

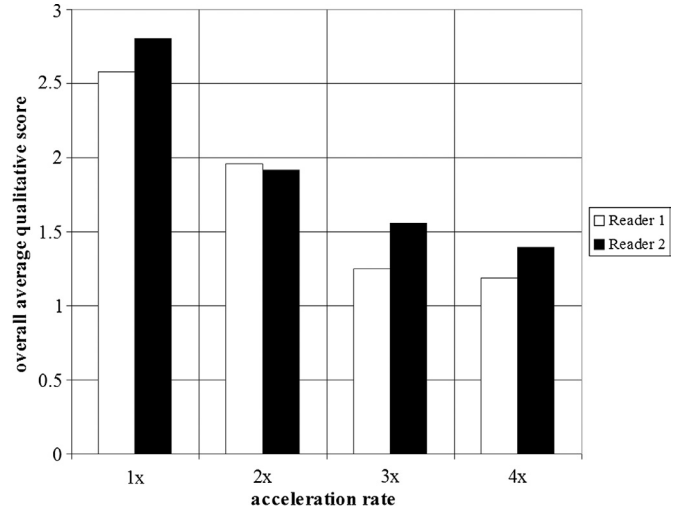

FIGURE 7. Overall average qualitative scores of the T2-FLAIR images for each reader. The score was calculated as an average of the image feature scores, averaged over the 10 patients and 2 image slices per patient.

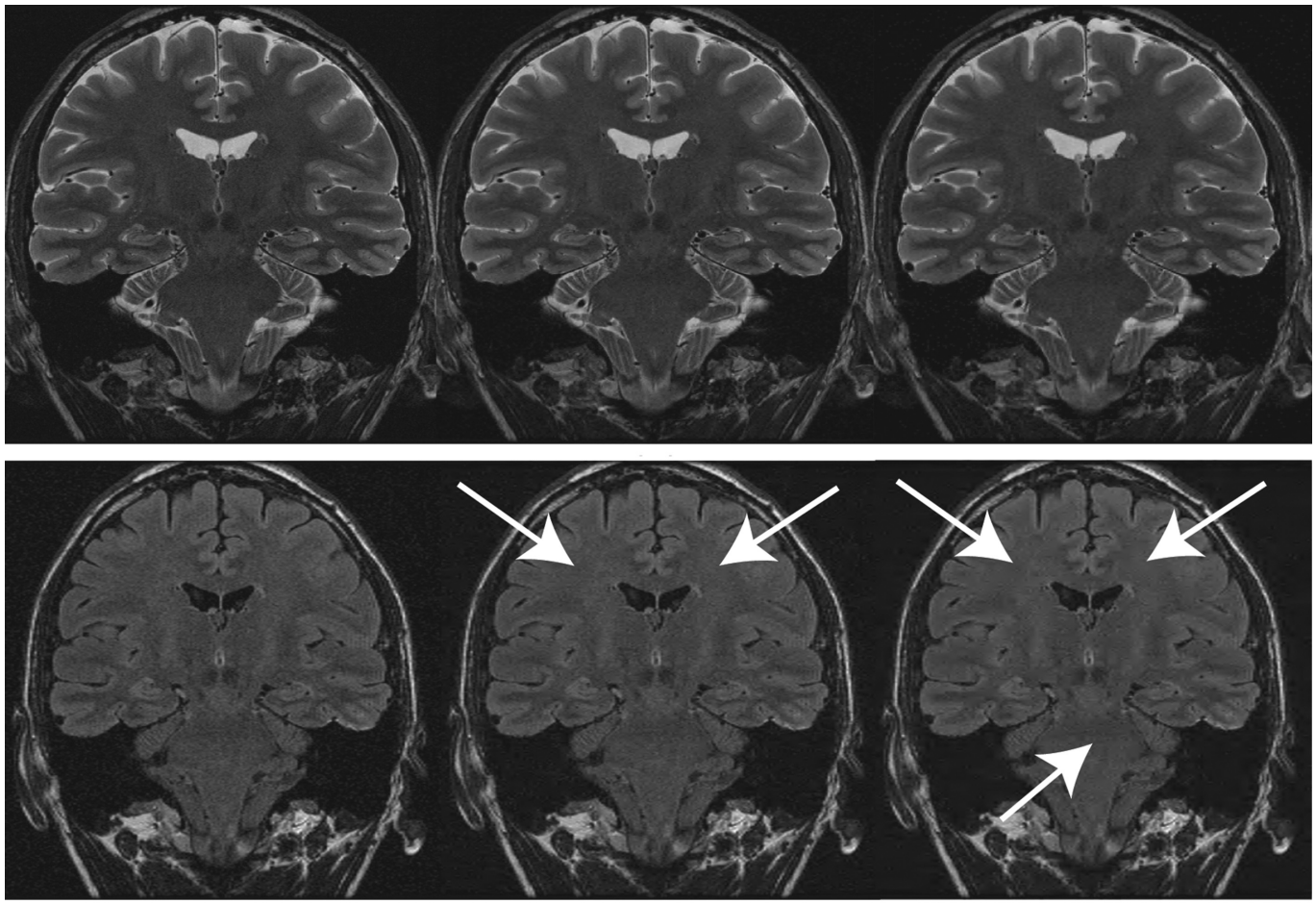

FIGURE 8. Images formed using a fractional amount of the available DB-4 wavelet coefficients. For each image, a fraction of the highest magnitude DB-4 wavelet coefficients was used to construct the image, with the other coefficients being set to 0. Top row: T2-SE; bottom row: T2-FLAIR. A, All DB-4 coefficients used; B, one-third of wavelet coefficients used; C, one-fifth of wavelet coefficients used. At one-third of the coefficients, the T2-FLAIR image suffers from noticeable blurring, which is amplified when only one-fifth of the coefficients are used (see white arrows). The effects on the T2-SE images are not as apparent. This indicates that images from the T2-SE sequence are relatively more compressible than the images from the T2-FLAIR sequence, which may explain why the qualitative scores were better for the T2-SE sequence for a fixed acceleration factor.

as well. This study used an iterative process that relied on neuroradiologist feedback to establish the sampling pattern and regularization parameter. This process would become unfeasible if CS were applied to an entire protocol, rather than just 2 sequences as in this work. A structured approach to choosing these parameters, as well as the sparsifying basis, must be developed before CS appears in routine clinical protocols.

CONCLUSION

This work has provided an investigation into the value of CS in clinical magnetic resonance neuroimaging. Image ringing and blurring were identified as 2 primary image artifacts that would hinder the ability to accurately diagnose pathology. Qualitative scores at up to 10 anatomical regions have shown that 2×-accelerated data acquisition is possible for those sequences with higher native spatial resolution. The integration of complementary acceleration techniques, such as parallel imaging, will allow for further acceleration and a need for a new analysis of artifacts.

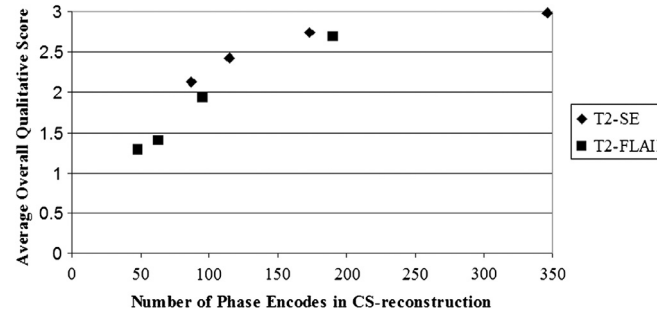

FIGURE 9. Overall average qualitative score, averaged over the 2 readers, as a function of the absolute number of phase-encoding lines used in the reconstruction. This is in contrast to traditionally reported results that use acceleration factor as the independent variable. There appears to be dependence of the qualitative score on the absolute number of phase encodes, regardless of the fully sampled acquisition size.

ACKNOWLEDGMENTS

The authors thank Mr Sam Valencerina for his help in acquiring the data at USC Healthcare Consultation Center II.

REFERENCES

1. Nishimura D. *Principles of Magnetic Resonance Imaging*. Stanford, CA: Stanford University; 1996.
2. Buxton R. *Introduction to Functional Magnetic Resonance Imaging: Principles and Techniques*. New York, NY: Cambridge University Press; 2002.
3. Donoho D. Compressed sensing. *IEEE Trans Inf Theory.* 2006;52:1289–1306.
4. Candes E, Romberg J, Tao T. Robust uncertainty principles: exact signal reconstruction from highly incomplete frequency information. *IEEE Trans Inf Theory.* 2006;52:489–509.
5. Lustig M, Donoho D, Pauly J. Sparse MRI: the application of compressed sensing for rapid MR imaging. *Magn Reson Med*. 2007;58:1182–1195.
6. Gamper U, Boesiger P, Kozerke S. Compressed sensing in dynamic MRI. *Magn Reson Med*. 2008;59:365–373.
7. Kim Y, Narayanan S, Nayak K. Accelerated three-dimensional upper airway MRI using compressed sensing. *Magn Reson Med*. 2009;61:1434–1440.
8. Ajraoui S, Lee K, Deppe M, et al. Compressed sensing in hyperpolarized 3He Lung MRI. *Magn Reson Med*. 2010;63:1059–1069.
9. Vasanawala S, Alley M, Hargreaves B, et al. Improved pediatric MR imaging with compressed sensing. *Radiology.* 2010;256:607–616.
10. Reichert M, Morelli JN, Runge VM, et al. Contrast-enhanced 3-dimensional SPACE versus MP-RAGE for the detection of brain metastases: considerations with a 32-channel head coil. *Invest Radiol*. 2013;48:55–60.
11. Park J, Kim J, Yoo E, et al. Detection of small metastatic brain tumors: comparison of 3D contrast-enhanced whole-brain black-blood imaging and MP-RAGE imaging. *Invest Radiol*. 2012;47:136–141.
12. Pruessmann K, Weiger M, Scheidegger M, et al. SENSE: sensitivity encoding for fast MRI. *Magn Reson Med*. 1999;42:952–962.
13. Gauvrit J, Law M, Xu J, et al. Time-resolved MR angiography: optimal parallel imaging method. *Am J Neuroradiol*. 2007;28:835.
14. Yudilevich E, Stark H. Spiral sampling in magnetic resonance imaging-the effect of inhomogeneities. *IEEE Trans Med Imaging*. 1987;6:337.
15. Kim Y, Nielsen J, Nayak K. Automatic correction of echo-planar imaging (EPI) ghosting artifacts in real-time interactive cardiac MRI using sensitivity encoding. *J Magn Reson Imaging*. 2008;27:239.
16. Liang D, Liu B, Wang J, et al. Accelerating SENSE using compressed sensing. *Magn Reson Med*. 2009;62:1574–1584.
17. Roemer P, Edelstein W, Hayes C, et al. The NMR phased array. *Magn Reson Med*. 2005;16:192–225.
18. Candes E, Tao T. Near-optimal signal recovery from random projections: universal encoding strategies? *IEEE Trans Inf Theory.* 2006;52:5406–5425.